02,05,13,12

An increase in the critical current of superconducting composites upon implantation of iron ions

© I.A. Rudnev[1,2], A.I. Podlivaev[1,3], D.A. Abin[1], S.V. Pokrovskii[1,2], A.S. Starikovskii[1], R.G. Batulin[2], P.A. Fedin[4], K.E. Prianishnikov[1,4], T.V. Kulevoy[4]

[1] National Research Nuclear University „MEPhI“, Moscow, Russia
[2] Kazan Federal University, Kazan, Russia
[3] Research Institute of Problems in the Development of Scientific and Educational Potential of Young People, Moscow, Russia
[4] National Research Center „Kurchatov Institute“, Moscow, Russia

E-mail: IARudnev@mephi.ru

Received November 30, 2022
Revised November 30, 2022
Accepted December 6, 2022

The results of studying the effect of ion irradiation (Fe^{2+} $E = 5.6$ MeV) in the modes of creating radiation defects and implantation on the critical current of high-temperature superconducting (HTS) composites are presented. An analysis was made of both the integral critical current obtained from measurements of the total magnetization of the samples and the local critical current determined from the data of scanning Hall magnetometry. It is shown that at the same ion fluence $\Phi = 2 \cdot 10^{13}$ cm^{-2}, an increase in the critical current J_c is observed in the ion implantation regime, while in the regime of radiation defects, a slight drop in J_c is observed. This circumstance indicates an enhancement of pinning due to the additional magnetic interaction of Abrikosov vortices with magnetic ions implanted in the HTS layer.

Keywords: high-temperature superconductor, irradiation, radiation defects, critical current, magnetization.

DOI: 10.21883/PSS.2023.03.55577.540

1. Introduction

Modern HTS composites of the second generation in the form of a thin HTS layer of $\sim 1-2\,\mu$m applied using a set of intermediate buffer layers on a metal substrate [1] are becoming more common in various electrical engineering and power industry devices. HTS composites have high critical current densities in strong magnetic fields, which makes them a promising material for use in superconducting magnetic facilities of the MEGA-science class (Large Hadron Collider (LHC), NICA accelerator, ITER project, etc.). HTS composites are used in other applications that require high densities of the critical current J_c, for example, in frictionless bearings based on a combination of permanent magnets and superconducting magnetic systems, which makes it possible to avoid tribological problems at cryogenic temperatures [2,3]. In [4–7] the possibility was shown to effectively replace permanent magnets with a stack of HTS tapes, which can be magnetized by a short-time exposure to an external magnetic field after which stacks keep the remanence magnetization for a long period of time. In [8] the possibility is shown to create a scalable bearing using HTS tapes.

Despite significant advances in the creation of HTS composites with high critical currents and their high uniformity along the piece length [9], different laboratories continue investigations aimed at the search for further increase of the critical current. One of such technique is the introduction of non-superconducting phase nanoinclusions into the superconducting matrix, which play, under certain conditions, the role of additional artificial centers of pinning and result in a critical current increase. The nanoparticles should meet the following two main criteria: first, they should not decrease significantly the critical temperature T_c, second, their typical size should be comparable with the coherence length. The most frequently used for this purpose are oxides of four-valence metals: M = Zr, Hf, Ce, Ti and Sn. They form islets of $BaMO_3$ perovskite of phases in the *Re*BCO matrix [10,11] (*Re* — atoms of rare-earth elements). The most commonly used are barium stannates and zirconates. In particular, in [12,13] it was shown that nanoparticles of $BaZrO_3$ are very promising as candidates for inert centers of pinning. Investigations focused on the creation of artificial centers of pinning based on nanoadditives were carried out for HTS tapes produced by different methods: pulsed laser deposition [14–16], liquid delivery metal-organic precursors for the chemical vapor deposition [17,18], metal-organic compounds for the chemical vapor deposition [10,11,19–23]. Along with monoadditives, a method of structure creation with a combination of point and columnar defects was considered [24]. A well-known

combination of these artificial centers of pinning are $BaZrO_3$ and Y_2O_3 [25,26], as well as $BaSnO_3$ [27].

As a result of investigations, it was shown that inclusions of $BaZrO_3$ in HTS thin films are assembled in correlated structures in the form of columnar defects that work well as centers of pinning in the perpendicular magnetic field [15,19–21]. Similar studies were conducted for $BaSnO_3$. A growth of critical current in the perpendicular field was shown, however a decrease in this current is observed in a field parallel to the plane of tape [11,27]. In [20,21] authors investigated in detail the effect of concentration of $BaZrO_3$ inclusions on magnetic and electric transport properties of HTS tapes of the second generation produced by the MOCVD method. It was shown that the optimum content of $BaZrO_3$ is about 5% mol. Thus, in [17] a technique was proposed to increase the critical current in HTS tapes with $BaZrO_3$ nanoinclusions by soaking the sample at intermediate temperatures in the process of crystallization by the MOD method. The artificial centers of pinning based on $BaZrO_3$ have the highest effect on HTS properties at low temperatures and strong magnetic fields [28]. Nevertheless, the improvement of the pinning effect in HTS with an addition of $BaZrO_3$ is noticeable at more higher temperatures as well [29]. Also known are studies aimed at critical current increase through the creation of defects using an ultrashort laser impact [30].

An alternative method to create artificial centers of pinning is the use of irradiation. In practice, the irradiation with neutrons [31–38], protons [39], electrons [40], γ-quanta [41] and heavy ions [42] is used. In addition to the possibility of additional pinning centers creation at low concentration of defects, the irradiation technique is attractive due to the fact that using an ion irradiation with energies of about $1-10\,\text{MeV}$ it is possible to create defect concentrations that significantly change the critical current and critical temperature up to the complete loss of superconductivity. In a recent study [43] we have demonstrated a drastic drop of critical temperature and critical current under the irradiation of HTS composites with Cu ions with an energy of $E = 6.3\,\text{MeV}$.

However, the irradiation not always has a destructive effect on superconducting characteristics. Studies of the effect of irradiation with heavy inert gas ions [44,45] show some growth of the critical current at low fluences followed by a monotonous decrease down to the complete loss of superconducting properties even at a fluence of $\sim 10^{13}\,\text{m}^{-2}$. As studies show, the radiation resistance of HTS tapes to the irradiation by $^{132}Xe^{27+}$ (167 MeV), $^{132}Xe^{27+}$ (80 MeV) and $^{84}Kr^{17+}$ (107 MeV) is $1\cdot 10^{12}\,\text{cm}^{-2}$, $3.5\cdot 10^{13}\,\text{cm}^{-2}$ and $1\cdot 10^{13}\,\text{cm}^2$, respectively. Also, investigations were carried out with the use of ions of oxygen [47–49], zirconium [50], lead [51]. It was shown that exposing to oxygen ions beam may increase the critical current by 2 times in the fields of about 5T

However, any type of irradiation creates nonmagnetic defects in the superconducting material. At the same time, it was shown both theoretically and experimentally that magnetic effects can amplify the pinning due to the additional electromagnetic interaction between Abrikosov vortices and magnetic moment of the defect [52–57].

This study investigates experimentally the possibility of radiation-induced creation of a nonuniform profile of density of the critical superconducting current in a HTS tape. First of all, the interest in this subject is caused by the possibility to create in both an individual tape and in a stack of HTS tapes the non-superconducting regions by irradiation. They can become pinning centers of Abrikosov vortices and, as a consequence, result in an increase in the critical transport current of the tape. The advantage of irradiation of stacks of HTS tapes is due to a) the lack of cracking in the fragile layer of ceramic superconductor, b) the lack of damages to the protective layer of the tape and c) the possibility to form in the desired region a correlated change in the superconducting characteristics of all HTS tapes of the stack.

In the first part of this study the effect of uniform irradiation of a HTS tape with iron ions on the critical current and critical temperature of the superconductor is investigated. The investigation will be carried out by magnetometer methods that make it possible to determine the total magnetization of the sample at different radiation doses and in a wide range of temperatures. The influence of implanted magnetic Fe^{2+} ions on the critical current of HTSC composites is presented We shall show that the implanted ions of iron increase the critical current of HTS composites, while the radiation-induced defects in a similar fluence do not result in a significant growth of J_c. This fact is indicative of an additional pinning arising due to the magnetic nature of the ions.

In the second part of the study the spatial distribution of superconducting current density will be investigated by scanning Hall magnetometry at a temperature of liquid nitrogen for different characters of the non-uniform irradiation.

2. Experiment

2.1. Samples for irradiation

We used as samples the tape-type HTS composites of the second generation serially produced by S-Innovations. These composites are a thin (about $1-2\,\mu\text{m}$) HTS layer of $GdBa_2Cu_3O_{7-x}$ applied on a flexible substrate made of Hastelloy C-276 alloy with a thickness of $60\,\mu\text{m}$, with the use of several buffer layers. As a rule, the HTS layer is covered by a layer of silver and all the composite is covered by copper. The critical temperature of HTS tape samples is $T_c \sim 90\,\text{K}$, their critical current is $I_c \sim 150\,\text{A}$ at a tape width of 4 mm. In our investigations we used tapes without and with silver coating with a thickness of $1.5\,\mu\text{m}$. Parameters of these tapes are close to appropriate characteristics of the tapes studied in [58,59]. In all cases the copper coating was removed from the composite area exposed by the irradiation.

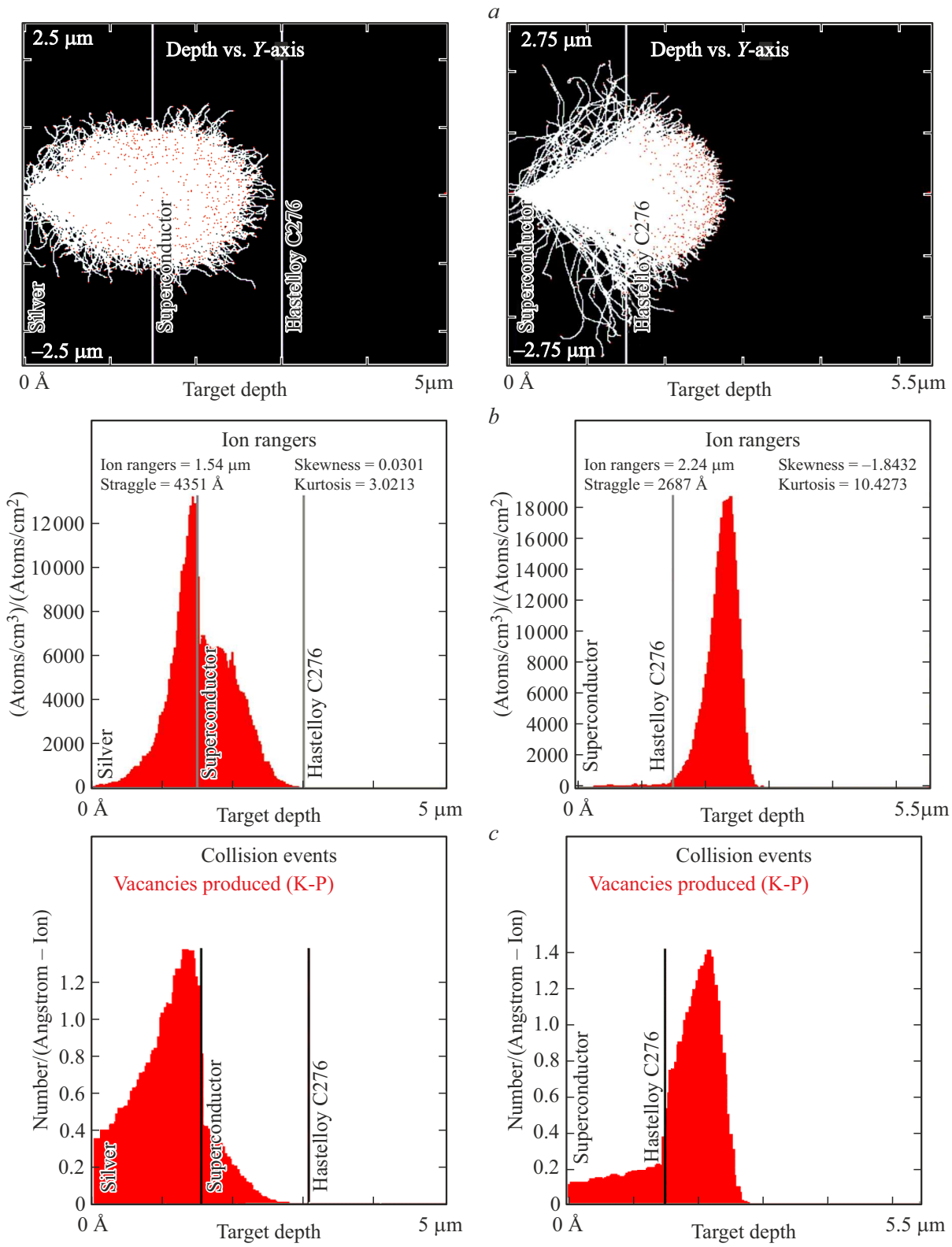

Figure 1. Profiles of radiation-induced damage in vertical direction of the sample with a 1.5 μm thick silver layer (left column) and without the silver layer (right column). Path of Fe ions flying through the layers of the tape (*a*). Distribution of Fe ions inside the sample (*b*). Distribution of density of vacancies inside the sample (*c*).

2.2. Calculation of defect formation modes

Due to the high cost of working time of the accelerator, the modes of irradiation were calculated in advance using the SRIM (Stopping and Range of Ions in Matter [60]) software package. We planned to irradiate HTS composites with Fe^{2+} ions with an energy of $E = 5.6$ MeV. Calculation results for the radiation-induced damage of the irradiated area of a sample with a silver layer thickness of $1.5\,\mu$m and without silver coating are shown in Fig. 1.

It can be seen from Fig. 1, that there is an implantation of iron ions into the HTS layer in the presence of the silver coating, while the absence of the silver coating results in the iron ions implantation into the substrate and only radiation-induced defects in the HTS layer are created.

The detailed experimental determination of the concentration of radiation-induced defects in the vertical direction requires special labor-intensive methods [59] and is beyond the scope of this study. In this study we just note the presence of implanted ions and radiation-induced vacancies in the superconducting layer with the selected type of irradiation, as well as determine the change in superconductor characteristics under the effect of these defects.

2.3. Ionic irradiation

HTS composites were irradiated by Fe^{2+} ions with an energy of $E = 5.6$ MeV (101 keV per nucleon) in a TIPr-1 accelerator in the Institute for Theoretical and Experimental Physics of the „Kurchatov Institute“ National Research Center. The pulse current of a Fe^{2+} ion beam on the sample area in this mode is $20\,\mu$A with a current density of $12\,\mu$A/cm^2. Mean rate of fluence achievement is $3.2 \cdot 10^{13}$ ions/cm^2 for one hour. Several samples were irradiated simultaneously. Some of the samples had an uncovered HTS layer, which allowed ions to freely affect the HTS structure creating radiation defects (Fig. 2). Other samples had their HTS layers covered by a layer of silver with a thickness of $1.5\,\mu$m (thickness of the silver layer was tested by a NTEGRA atomic-force microscope). In the previous section it was shown, that the use of silver layer as a decelerator of ions resulted in the implantation of Fe ions into the HTS layer.

One of problems in case of this format of irradiation is that the frontal uniformity of the radiation-induced damage to the irradiated area needs to be controlled. The technique of appropriate control is described below in section 3.2.

2.4. Measurement of the magnetization and calculation of the critical current

Initial (before irradiation) samples of HTS tapes and irradiated samples of HTS tapes were measured by a PPMS-9 setup. For the measurement, the samples were cut out in the form of circle with a diameter of 3 mm. Quality of the cut was tested using magneto-optical visualization (see [43] for further details). The local distribution of critical current was measured by the method of scanning Hall magnetometry.

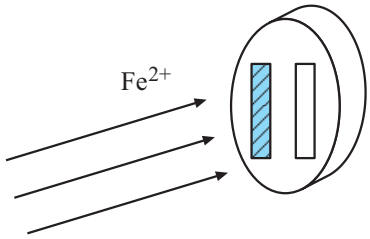

Figure 2. Schematic diagram of samples irradiation through a mask. Shaded region — sample with silver coating, unshaded region — sample without silver coating. Both samples were irradiated simultaneously with the same fluence.

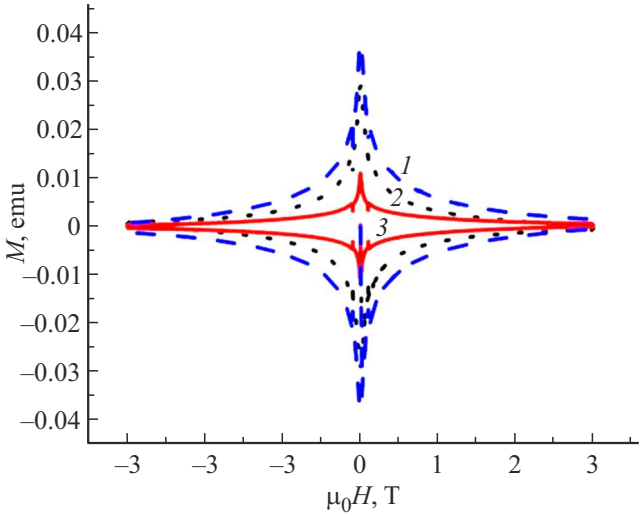

Figure 3. Magnetization curves for samples at a temperature of $T = 77$ K: *1* — sample irradiated through a silver layer (in the mode of implantation) with a fluence of $\Phi = 2 \cdot 10^{13}$ cm^{-2}, *2* — sample of initial tape without modifications, *3* — sample with directly irradiated superconducting layer (in the mode of creation of radiation-induced defects) with a fluence of $\Phi = 2 \cdot 10^{13}$ cm^{-2}.

3. Experimental findings and discussion

3.1. Integral measurements of magnetization

Fig. 3 shows magnetization curves for the initial sample, as well as for samples irradiated in the mode of implantation and in the mode of creation of radiation-induced defects. The conversion of the critical current from the magnetization curves demonstrates an increase in J_c in the implantation mode and a decrease in it in the mode of structural radiation-induced defects (Fig. 4). The increase in the critical current depends on the strength of the external applied field. Thus, without the field the growth of the critical current was approximately 30%, and in a field range of 1–2 T the increase was almost 100%.

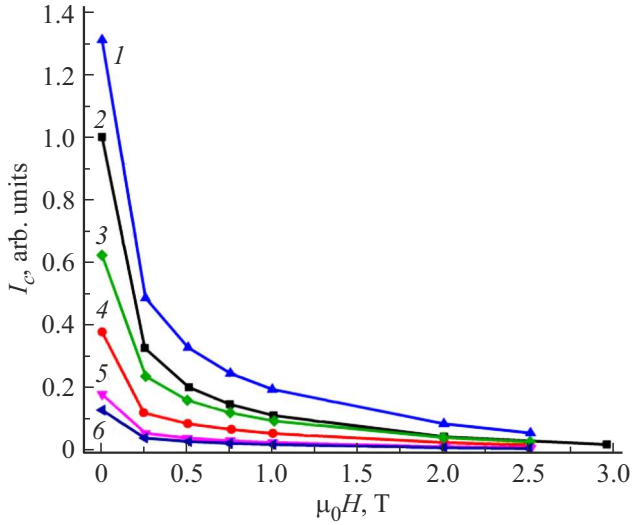

Figure 4. Normalized critical current as a function of external magnetic field strength for different samples at $T = 77$ K; *1* — sample irradiated through a silver layer with a fluence of $\Phi = 2 \cdot 10^{13}$ cm^{-2}, *2* — sample of the initial tape without modifications, *3* — sample irradiated through a silver layer with a fluence of $\Phi = 3 \cdot 10^{13}$ cm^{-2}, *4* — sample with uncovered superconducting layer irradiated with a fluence of $\Phi = 2 \cdot 10^{13}$ cm^{-2}, *5* — sample with uncovered superconducting layer irradiated with a fluence of $\Phi = 3 \cdot 10^{13}$ cm^{-2}, *6* — sample with uncovered superconducting layer irradiated with a fluence of $\Phi = 5 \cdot 10^{13}$ cm^{-2}.

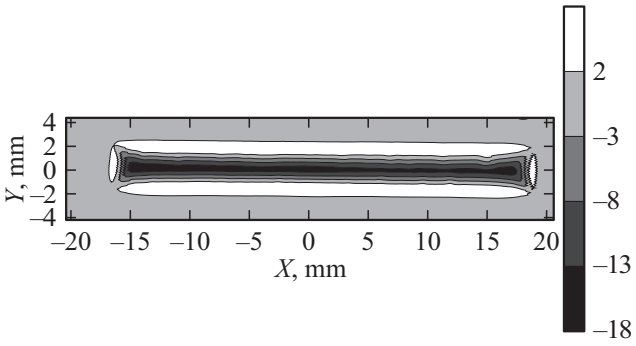

Figure 5. Level lines of the profile of residual magnetic induction B_Z (mT) in the (X, Y) plane. Distance between the lines is 5 mT. Tape sample № 1.

3.2. Local measurements of the critical current

The above-presented hysteresis loops of the magnetization of irradiated HTS samples give us integral characteristics of superconducting currents. For a detailed studying of the current-carrying characteristics of the irradiated HTS tapes, as well as to control the frontal uniformity of the irradiation, we used scanning Hall magnetometry of the obtained samples. All the studied samples were produced from one initial fragment of a serially manufactured $GdBa_2Cu_3O_{7-x}$-based tape by S-Innovations. Width of the tape was 4 mm. Structure of the tape under study was similar to that of the tapes studied in the previous section.

The local irradiation of the tape forms a non-uniform profile of defects in it that change the superconducting characteristics of the HTS sample. To determine the effect of irradiation, an information is needed on the initial non-uniformity of the tape caused by the imperfection of its manufacturing process. To determine the non-uniformity of critical current density in an unirradiated tape, the Hall magnetometry was used to determine the field of two-dimensional superconducting currents induced by an external magnetic field. Two fragments of the tape were taken as samples. Each fragment had a length of 35 mm. The samples were cooled to a temperature of liquid nitrogen, magnetized by NdFeB-based permanent magnets and after removal of the magnets the residual magnetic field was determined by the scanning Hall magnetometry. The scanning magnetometry has proven to be an effective method to estimate current-carrying characteristics of superconductors (see, for example, [61–63]. Based on the magnetometry data, the solution to the inverse problem of Biot-Savart-Laplace, as well as the application of model of critical state of superconductors [64,65] make it possible to determine the critical current of the superconductor in the region where the critical state is achieved. The Biot-Savart-Laplace law establishes the relation between currents with a density of $j(r)$ distributed in the V region and the magnetic field induction vector, $B(r)$, created by these currents.

$$B(r) = \frac{\mu_0}{4\pi} \int\limits_V \frac{j(r')(r - r')d^3r'}{|r - r'|^3}. \qquad (1)$$

The solution to inverse problem of Biot-Savart-Laplace is understood as the determination of $j(r)$ from integral equation (1) at a magnetic field induction $B(r)$ known from the data of scanning magnetometry.

Fig. 5 shows normal component $B_Z(X, Y)$ of the residual magnetic field of one of unirradiated samples (hereinafter referred to as „sample 1“). The measurement was carried out in the (X, Y) plane by a Hall sensor with a scanning step of 0.1 mm at a height of 0.3 mm from the sample surface. It can be seen in this figure, that the field away from the tape edges is nearly uniform. The are no signs of any defects. It is difficult to estimate the level of non-uniformity of the critical current without additional processing of the data presented in Fig. 5.

The dispersion of critical current density can be determined by solving the inverse problem of Biot-Savart-Laplace (1). Fig. 6 shows lines of currents in the sample obtained as a result of solving the inverse problem.

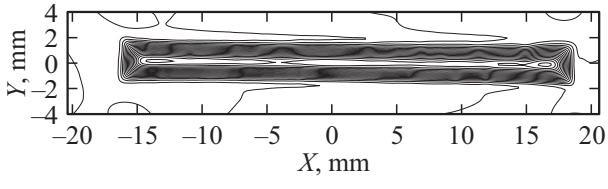

Figure 6. Lines of currents in the (X, Y) plane. One line corresponds to a current of 2 A. Tape sample № 1.

It can be clearly seen in this figure the boundaries of current domains (bend of current lines) near the left and right edges of the tape, which are typical for the magnetization of superconducting samples of rectangular shape (see, for example, review in [62]. To quantitatively estimate the dispersion of the residual current, Fig. 7 shows modulus of the induced current as a function of the X coordinate along the $Y = const$ line. For sample 1 the data is presented along two lines symmetric with respect to the central line of the tape and deviating from the central line by $+1$ and -1 mm, respectively. Also, the red bold line in Fig. 7 shows a similar dependence for sample 2 with a $+1$ mm deviation from the central line. Sample 2 is cut out of the same tape as sample 1. Sample 2 had the lowest amplitude of the residual magnetic field as compared to other samples taken from the same tape.

The comparison of data in Fig. 7 shows that local (at typical lengths of ~ 20 mm) deviations of the critical current density from its mean value are $\sim 4\%$. At larger distances the mean value of this parameter can vary adiabatically by not more than by 10%.

Also, based on the initial tape, samples № 3 and № 4 were made and irradiated by iron ions with an energy of 5.6 MeV. Frontal view of sample 3 is shown in Fig. 8.

Fig. 9 shows normal component $B_Z(X, Y)$ of the residual magnetic field of irradiated sample 3.

A poorly resolved light-color contour can be seen in Fig. 9 in the irradiated region, however it is hardly possible to quantitatively determine the change in superconducting characteristics of the sample on the basis of visual perception of this figure. Lines of superconducting current recovered from the solution of equation (1) are shown in

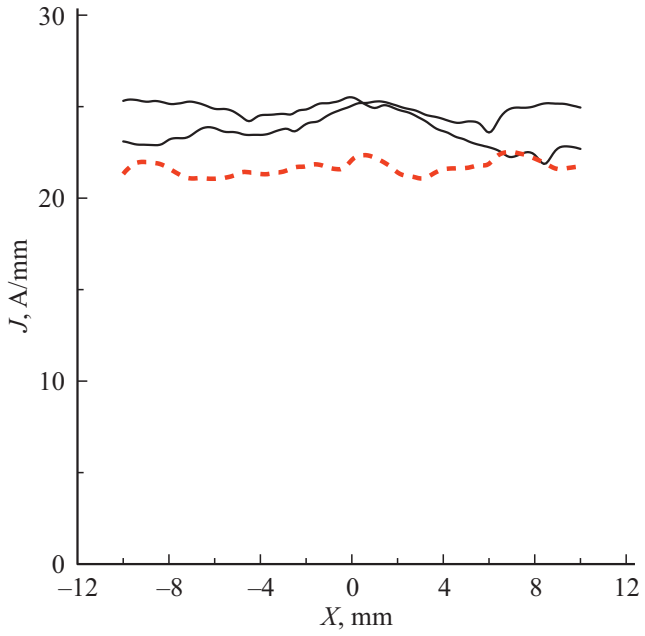

Figure 7. Density of induced current $J(X)$ along the lines $Y = \pm 1$ mm for tape sample № 1 (black solid lines) and along the line $Y = +1$ mm for tape sample № 2 (bold dashed red line).

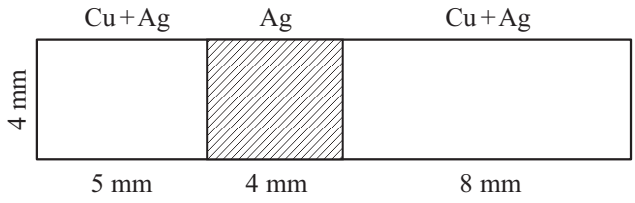

Figure 8. Frontal view of sample 3. The unshaded regions of the sample have copper and silver protective coatings. The copper protective layer is removed from the shaded region, however the silver protective layer is still there, and only this region is exposed to further irradiation by iron ions through a mask.

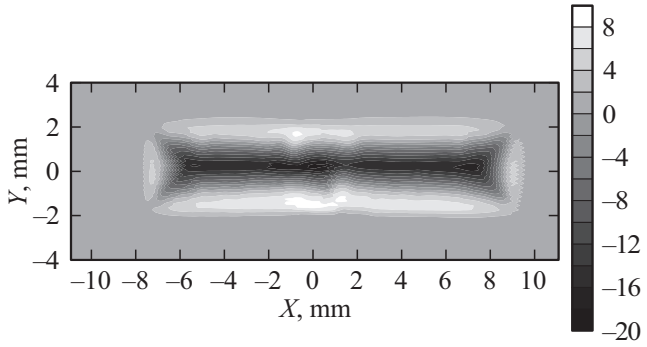

Figure 9. Level lines of the profile of residual magnetic induction B_Z (mT) in the (X, Y) plane. Distance between the lines is 2 mT. Tape sample № 3. The middle of the irradiated region (4×4 mm) has the following coordinate: $X \sim -0.5$ mm.

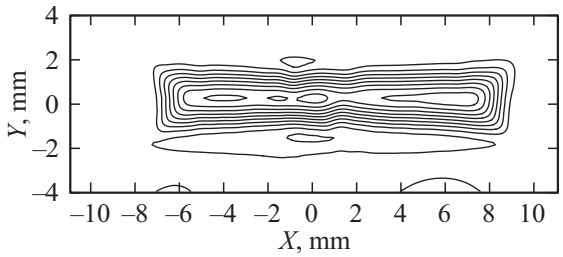

Figure 10. Lines of currents in the (X, Y) plane. One line corresponds to a current of 4 A. Tape sample № 3. The middle of the irradiated region (4×4 mm) has the following coordinate: $X \sim -0.5$ mm.

Fig. 10. The density of induced current is proportional to the density of currents, and a noticeable densification of current lines can be seen in the irradiated region in Fig. 10. The nonmonotonous dependence of the integral critical current on the irradiation dose was presented in the previous section, the scanning Hall magnetometry confirms the growth of critical current density at low doses of irradiation.

The increase in the critical current density is related to the microscopic non-uniformities in the distribution of radiation-induced defects, which are pinning centers for Abrikosov vortices in a superconductor. Fig. 11 shows density of the

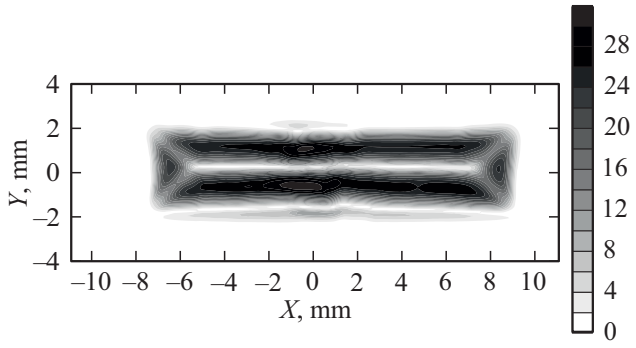

Figure 11. Density of the induced two-dimensional current (A/mm) in the (X, Y) plane. Tape sample № 3. The middle of the irradiated region (4×4 mm) has the following coordinate: $X \sim -0.5$ mm.

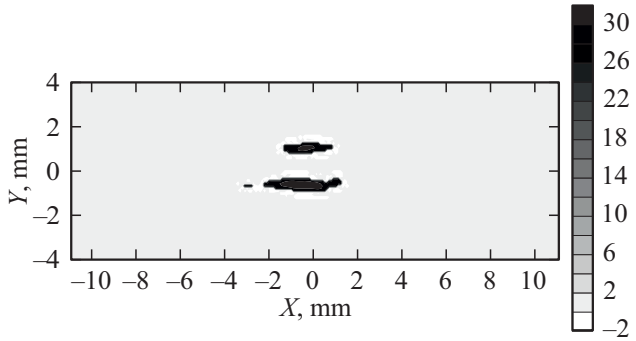

Figure 12. Contrast image of the density of induced current in the (X, Y) plane. Regions of the plane are shown, where the current density is within the interval of $28 < J < 30$ A/mm. Tape sample № 3. The middle of the irradiated region (4×4 mm) has the following coordinate: $X \sim -0.5$ mm.

induced current in sample № 3. The comparison of data in Fig. 7 and 11 shows that the peak current density is higher in the irradiated sample 3. To highlight the regions with increased density, a contrast image of the current density is presented in Fig. 12.

It can be seen in this figure, that increased currents are only observed in the region exposed to the irradiation. Also, it is worth to note a certain non-uniformity arisen after the irradiation: the lower region of increased current in the zone of irradiation is larger as compared to the upper region, however the size of this non-uniformity is small and can be a consequence of the process imperfection when manufacturing the initial section of the HTS tape. At the same time, the increase in critical current in the upper and lower regions as compared to the unirradiated part of the sample is in no doubt. The density of induced current $J(X)$ along the lines of $Y = -0.6$ and 1.1 mm for tape sample № 3 is shown in Fig. 13. It can be seen in this figure, that the mean current density outside the irradiated region matches the data presented in Fig. 7 (~ 25 A/mm), and inside the irradiated region it is in the range of 26–32 A/mm. Thus, the increase in the induced current stimulated by the irradiation is considerably higher than the dispersion of the current density in unirradiated samples 1 and 2.

On the following irradiated sample (№ 4) both copper and silver protective layers were removed from the irradiated regions. Iron ions were falling directly on the superconducting film. Shape of the irradiated sample № 4 is shown in Fig. 14.

Fig. 15 shows distribution of the normal component of the residual magnetic induction vector in the (X, Y) plane.

Fig. 16 shows lines of induced currents in sample № 4. In this figure, the structure of current lines in unirradiated regions, as expected, has a form of closed circles with clearly distinguished domain structure. However, the character of current lines in the irradiated region is unusual.

In the major portion of the left and right boundaries of both irradiated regions there is no longitudinal component of the J_X current. This follows from the fact, that the near-boundary lines of current in the irradiated region are parallel to the irradiation boundary. Such an effect can arise in the case of full (stronger than average over the irradiated region) suppression of the superconductivity in a narrow band along the boundaries. Indeed, it can be clearly seen in Fig. 17, where the modulus of current along the longitudinal line of $Y = -0.5$ mm is shown, that there is a drop of this parameter near the boundaries of irradiated regions ($X \sim -9$, -5 and 6, 10 mm). A similar effect is explained in [58] as follows. In the case, when the density of the critical current has a discontinuity at the boundary of the irradiated and unirradiated regions, the component of induced current J_Y also has a stepwise change at this boundary. In this case, from the solution to the Biot-Savart-Laplace equation follows a sharp increase in amplitude of the magnetic field, including that in the boundary band of the irradiated region. The high magnetic field caused by the currents of unirradiated region suppresses the weak superconductivity in the adjacent irradiated region.

It is worth noting that similar effects of radiation-induced formation of magnetic field concentrators hypothetically can be used in numerous technical applications where a highly non-uniform magnetic field is needed (systems with magnetic levitation, filtration of ferromagnetic dust, dressing of ores of ferromagnetic elements, etc.). The advantage of radiation-induced formation of a non-uniform profile of critical current density before the chemical etching or laser damage consists in the absence of mechanical damages to the protective layer and fragile HTS film.

The asymmetry of current lines pattern with respect to the central line of the tape in both irradiated regions is indicative of a weak yet clearly diagnosable non-uniformity of the density in the direction of the Y axis. The simultaneous arising of this non-uniformity in both irradiated regions makes it possible to relate it to the varying, smoothly changing intensity of the radiation impact in the Y frontal direction.

It is worth to note one more feature of the irradiation effect on the irradiated sample. In Fig. 17, in unirradiated parts a strong dispersion of the current density is observed,

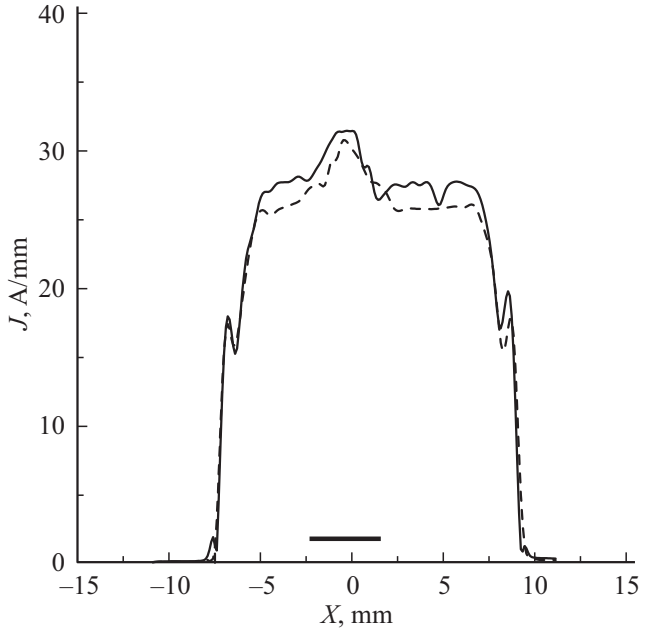

Figure 13. Density of the induced current $J(X)$ along the lines of $Y = -0.6$ mm (solid line) and $Y = 1.1$ mm (dashed line). Sample № 3. The bold section of the line near the X axis shows the irradiated region.

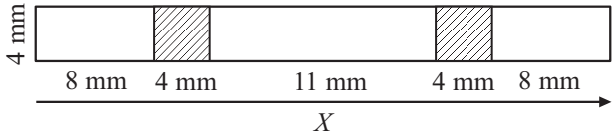

Figure 14. Shape and dimensions of sample № 4. In the shaded regions protective layers are removed. Only these regions were exposed to the irradiation through appropriate mask.

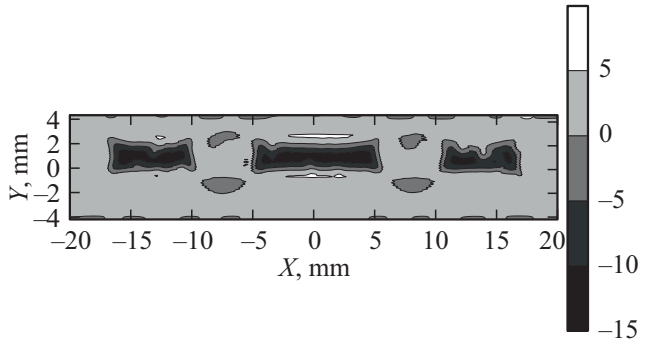

Figure 15. Level lines of the profile of residual magnetic induction B_Z (mT) in the (X, Y) plane. Distance between the lines is 5 mT. Tape sample № 4.

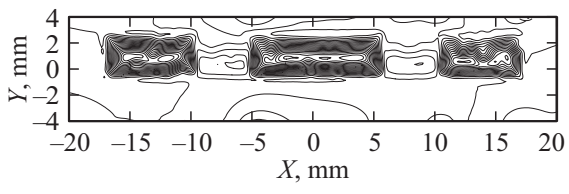

Figure 16. Lines of induced currents in sample № 4. One line corresponds to a current of 2 A.

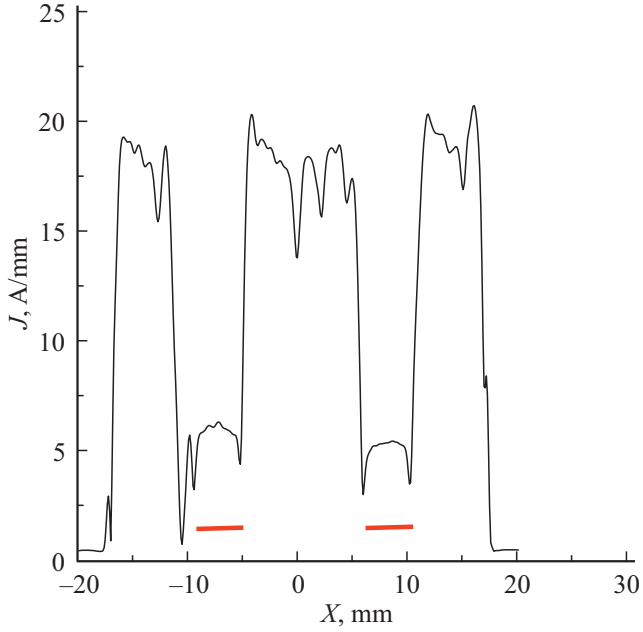

Figure 17. Density of the induced current $J(X)$ along the line of $Y = -0.5$ mm. Sample № 4. Bold red lines near the X axis show the irradiated regions.

the dependence of $J_c(X)$ is „rough“, while in the irradiated parts (shown by the red bar along the X axis) this dependence is smooth enough, without sharp short-wave spikes. Such a feature suggests that the irradiation with ions has a disproportionately strong suppression effect on the superconductivity in the regions where density of the critical current is not very high and has a considerably weaker effect on the initially more defective regions with poor superconducting characteristics, which results in decrease in the „roughness“ of the $J_c(\mathrm{X})$ curve. The explanation of this feature requires a separate detail consideration and in this study we are limited only by the establishment of the experimental fact — the smoothing of initial non-uniformities of the HTS films due to ionic irradiation.

4. Conclusion

In this study the possibility to increase the critical current in HTS composites by implanting magnetic ions into the superconducting layer is shown. The increase of critical current density with implantation of magnetic ions is higher than for the case of non-magnetic radiation-induced defects is shown that the scanning Hall magnetometry has a sufficient sensitivity to determine the non-uniformity of the radiation effect on the superconducting film with a typical size of a few millimeters and created by ion accelerator.

It is found that a strong suppression of superconducting properties of an HTS tape by radiation results in a disproportionately strong decrease in the critical current density. Such disproportion occurs in the regions where initially this density was the most high, while low current

density regions of the HTS material are affected to a less extent.

Funding

The study was supported by the Russian Foundation for Basic Research within the research project № 20-08-00811 (I.A. Rudnev, S.V. Pokrovsky, S.A. Starikovsky — the experimental part of the study), as well as supported by the Russian Foundation for Basic Research and „Rosatom" State Corporation with the research project No. 20-21-00085 (D.A. Abin, A.I. Podlivaev — the theoretical part of the study).

Conflict of interest

The authors declare that they have no conflict of interest.

References

[1] Tokonesushchiye lenty vtorogo pokoleniya na osnove vysokotemperaturnykh sverkhprovodnikov /Eds. A. Goyal. Isd-vo LKI, M. (2009), 432 p. (in Russian).
[2] I. Valiente-Blanco, E. Diez-Jimenez, C. Cristache, M.A. Alvarez-Valenzuela, J.L. Perez-Diaz. Tribology Lett. June (2013). DOI: 10.1007/s11249-013-0204-0 https://www.researchgate.net/publication/256277739
[3] F. Antoncik, M. Lojka, T. Hlasek, V. Bartunek, I. Valiente-Blanco, J.L. Perez-Diaz, O. Jankovsky. Supercond. Sci. Technol. **33**, *4*, 045010 (2020).
[4] I.A. Rudnev, A.I. Podlivaev. IEEE Trans. Appl. Supercond. **26**, *4*, 8200104 (2016).
[5] A.I. Podlivaev, I.A. Rudnev. FTT **63**, *10*, 1514 (2021). (in Russian).
[6] A.I. Podlivaev, I.A. Rudnev. FTT **64**, *2*, 167 (2022). (in Russian).
[7] A.I. Podlivaev, S.V. Pokrovskii, S.V. Veselova, I.V. Anishchenko, I.A. Rudnev. IEEE Trans. Appl. Supercond. **31**, *5*, 4601505 (2021).
[8] M. Osipov, I. Anishenko, A. Starikovskii, D. Abin, S. Pokrovskii, A. Podlivaev, I. Rudnev. Supercond. Sci. Technol. **34**, *3*, 035033 (2021).
[9] „S-Innovations" Company https://www.s-innovations.ru
[10] O.V. Boytsova, S.V. Samoilenkov, A.V. Vasiliev, A.R. Kaul, A.V. Kalinov, I.F. Voloshin. ECS Transact. **25**, 1185 (2009).
[11] S.V. Samoilenkov, A.R. Kaul, V.A. Amelichev, O.V. Boytsova. Supercond. Sci. Technol. **24**, 055003 (2011).
[12] H. Zhou, B. Maiorov, S.A. Baily, P.C. Dowden, J.A. Kennison, L. Stan, T.G. Holesinger, Q.X. Jia, S.R. Foltyn, L. Civale. Supercond. Sci. Technol. **22**, 085013 (2009).
[13] S.C. Wimbush, D. Walsh, S.R. Hall. Phys. C-Supercond. Appl. **470**, 373 (2010).
[14] H. Kobayashi, S. Ishida, K. Takahashi, M. Konishi, A. Ibi, S. Miyata, Y. Yamada, Y. Shiohara, T. Kato, T. Hirayama. Phys. C-Supercond. Appl. **445**, 625 (2006).
[15] K. Kaneko, K. Furuya, K. Yamada, S. Sadayama, J.S. Barnard, P.A. Midgley, T. Kato, T. Hirayama, M. Kiuchi, T. Matsushita, A. Ibi, Y. Yamada, T. Izumi, Y. Shiohara. J. Appl. Phys. **108**, 063901 (2010).
[16] A.P. Menushenkov, A.A. Ivanov, O.V. Chernysheva, I.A. Rudnev, M.A. Osipov, A.R. Kaul, V.N. Chepikov, O. Mathon, V. Monteseguro, F. d'Acapito, A. Puri. Supercond. Sci. Technol. **35** 065006 (2022).
[17] R. Teranishi, K. Konya, M. Inoue, Y. Sato, K. Kaneko, T. Izumi, S. Awaji. IEEE Trans. Appl. Supercond. **28**, 5, (2018).
[18] S.M. Choi, G.M. Shin, S.I. Yoo. Phys. C-Supercond. Appl. **485**, 154 (2013).
[19] A.P. Menushenkov, V.G. Ivanov, V.N. Chepikov, R.R. Nygaard, A.V. Soldatenko, I.A. Rudnev, M.A. Osipov, N.A. Mineev, A.R. Kaul, O. Matho. Supercond. Sci. Technol. **30**, 8 (2017).
[20] V.A. Maroni, A.J. Kropf. Supercond. Sci. Technol. **23**, 014020 (2010).
[21] V. Selvamanickam, A. Guevara, Y. Zhang, I. Kesgin, Y. Xie, G. Carota, Y. Chen, J. Dackow, Y. Zhang, Y. Zuev, C. Cantoni, A. Goyal, J. Coulter, L. Civale Supercond. Sci. Technol. **23**, 014014 (2010).
[22] N.M. Hapipi, K. Chen, A.H. Shaari, M.M.A. Kechik, K.B. Tan, K.P. Lim, O.J. Lee. J. Supercond. Nov. Magn. **32**, *5*, 1191 (2019).
[23] P. Prayoonphokkharat, P. Amonpattaratkit, A. Watcharapasorn. Appl. Phys. A Mater. Sci. Proc. **126**, *2*, 1 (2020).
[24] B. Maiorov, S. Baily, H. Zhou, O. Ugurlu, J. Kennison, P. Dowden, T. Holesinger, S. Foltyn, L. Civale. Nature Mater. **8**, 398 (2009).
[25] M. Sebastian, C. Ebbing, W. Zhang, J. Huang, H. Wang, S. Chen, B. Gautum, J. Wu, T. Haugan. Comparison study of the flux pinning enhancement of YBCO superconductor with BZO and BZO + Y_2O_3 mixed phase additions. In Proc. Int. Cryogenic Mater. Conf. (ICMC 2017). Madison, WI, USA (9–13 July, 2017). 012031 p.
[26] M. Pižl, O. Jankovský, P. Ulbrich, N. Szabó, I. Hoskovcová, D. Sedmidubský, V. Bartunek. J. Organomet. Chem. **830**, 146 (2017).
[27] V. Chepikov, N. Mineev, P. Degtyarenko, S. Lee, V. Petrykin, A. Ovcharov, A. Vasiliev, A. Kaul, V. Amelichev, A. Kamenev. Supercond. Sci. Technol. **30**, 124001 (2017).
[28] F. Rizzo. Supercond. Sci. Technol. **33**, 2 (2020).
[29] M. Kochat, R. Pratap, E. Galstyan, G. Majkic, V. Selvamanickam. IEEE Trans. Appl. Supercond. **29**, 4 (2019).
[30] S.V. Pokrovskii, O.B. Mavritskii, A.N. Egorov, N.A. Mineev, A.A. Timofeev, I.A. Rudnev. Supercond. Sci. Technol. **32**, *7*, 075008, 2019/06/06 (2019).
[31] J.S. Umezawa, G.W. Crabtree, J.Z. Liu, H.W. Weber, W.K. Kwok, L.H. Nunez, T.J. Moran, C.H. Sowers, H. Claus. Phys. Rev. B **36**, 7151 (1987).
[32] M.C.H.W.W.M. Eisterer, R. Fuger, M. Chudy, F. Hengstberger, H.W. Weber. Supercond. Sci. Technol. **23**, *1*, 014009 (2009).
[33] M. Chudy, R. Fuger, M. Eisterer, H.W. Weber. IEEE Transact. Appl. Supercond. **21**, *3*, 3162 (2011).
[34] R. Prokopec, D.X. Fischer, H.W. Weber, M. Eisterer. Supercond. Sci. Technol. **28**, *1*, 014005 (2014).
[35] M. Jirsa, M. Rames, I. Duran, T. Melısek, P. Kovac, L. Viererbl. Supercond. Sci. Technol. **30**, *4*, 045010 (2017).
[36] K.J. Leonard, F.A. List III, T. Aytug, A.A. Gapud, J.W. Geringer. Nucl. Mater. Energy **9**, 251 (2016).
[37] D.X. Fischer, R. Prokopec, J. Emhofer, M. Eisterer. Supercond. Sci. Technol. **31**, *4*, 044006 (2018).
[38] J. Emhofer, M. Eisterer, H.W. Weber. Supercond. Sci. Technol. **26**, *3*, 035009 (2013).
[39] B.M. Vlcek, H.K. Viswananthan, M.C. Frischherz, S. Fleshler, K. Vandervoort, J. Downey, U. Welp, M.A. Kirk, G.W. Crabtree. Phys. Rev. B **40**, 67 (1993).

[40] J. Giapintzakis, W.C. Lee, J.P. Rice, D.M. Ginsberg, I.M. Robertson, M.A. Kirk, R. Wheeler. Phys. Rev. B **45**, 10677 (1992).
[41] M.K. Hasan, J. Shobaki, I.A. Al-Omari, B.A. Albiss, M.A. Alakhras, K.A. Azez, A.K. El-Qisari, J.S. Kouvel. Supercond. Sci. Technol. **12**, 606 (1999).
[42] L. Civale, A.D. Marwick, T.K. Worthington, M.A. Kirk, J.R. Thompson, L. Krusin-Elbaum, Y.R. Sun, J.R. Clem, F. Holtzber. Phys. Rev. Lett. **67**, 648 (1991).
[43] I. Rudnev, D. Abin, S. Pokrovskii, I. Anishchenko, A. Starikovskii, M. Osipov, T. Kulevoy, P. Fedin, K. Pryanishnikov, R. Batulin, A. Kiiamov. IEEE Transact. Appl. Supercond. **32**, *4*, 8000905, June (2022).
[44] G. Mikhailova, L. Antonova, A. Troitskii, A. Didyk, V. Malginov, T. Demikhov, E. Suvorova. Phys. Status Solidi C **10**, *4*, 677 (2013).
[45] A.V. Troitskii, L.K. Antonova, T.E. Demikhov, V.A. Skuratov, V.K. Semina, G.N. Mikhailova. Physica C **572**, 1353631 (2020).
[46] E.I. Suvorova, P.N. Degtyarenko, I.A. Karateev, A.V. Ovcharov, A.L. Vasiliev, V.A. Skuratov, Ph.A. Buffat. J. Appl. Phys. **126**, 145106 (2019)
[47] N. Haberkorn, S. Suarez, P.D. Perez, H. Troiani, P. Granell, F. Golmar, S.H. Moon. Physica C **542**, *6*, 11 (2017).
[48] M. Leroux, K.J. Kihlstrom, S. Holleis, M.W. Rupich, S. Sathyamurthy, S. Fleshler, W.K. Kwok. Appl. Phys. Lett. **107**, *19*, 192601 (2015).
[49] S. Eley, M. Leroux, M.W. Rupich, D.J. Miller, H. Sheng, P.M. Niraula, L. Civale. Supercond. Sci. Technol. **30**, *1*, 015010 (2016).
[50] N. Haberkorn, S. Suarez, J.H. Lee, S.H. Moon, H. Lee. Solid State Commun. **289**, 51 (2019).
[51] I.A. Sadovskyy, Y. Jia, M. Leroux, J. Kwon, H. Hu, L. Fang, W.K. Kwok. Adv. Mater. **28**, *23*, 4593 (2016).
[52] A. Hoffmann, L. Fumagalli, N. Jahedi, J.C. Sautner, J.E. Pearson, G. Mihajlović, & V. Metlushko. Phys. Rev. B **77**, *6*, 060506 (2008).
[53] J.E. Villegas, K.D. Smith, L. Huang, Y. Zhu, R. Morales, & I.K. Schuller. Phys. Rev. B, **77**, *13*, 134510 (2008).
[54] J.I. Martín, M. Vélez, J. Nogués, I.K. Schuller. Phys. Rev. Lett. **79**, *10*, 1929 (1997).
[55] M.M. Al-Qurainy, A. Jones, S. Rubanov, S.A. Fedoseev, I. Rudnev, A. Hamood, A.V. Pan. Supercond. Sci. Technol. **33**, *10*, 105006 (2020).
[56] I.A. Golovchanskiy, A.V. Pan, S.A. Fedoseev, M. Higgins. Appl. Surf. Sci. **311**, 549 (2014).
[57] V.A. Kashurnikov, A.N. Maksimova, I.A. Rudnev. FTT **56**, *5*, 861 (2014).
[58] A.I. Podlivaev, I.A. Rudnev. FTT **64**, *3*, 319 (2022).
[59] A.I. Podlivaev, I.A. Rudnev. FTT **63**, *6*, 712 (2021).
[60] P. Biersack, L.G. Haggmark. Nucl. Instrum. Meth. Phys. Res. B **74**, 257 (1980). WWW.srim.org.
[61] S.J. Bending. Adv. Phys. **48**, *4*, 449 (1999).
[62] Ch. Jooss, J. Albrecht, H. Kuhn, S. Leonhardt, H. Kronmuller. Rep. Prog. Phys. **65**, 651 (2002).
[63] J.R. Kirtley. Rep. Prog. Phys. **73**, 126501 (2010).
[64] C.P. Bean. Phys. Rev. Lett. **6**, 250 (1962).
[65] C.P. Bean. Rev. Mod. Phys. **36**, 31 (1964).

Translated by Y.Alekseev